AIAA JOURNAL
Vol. 30, No. 11, November 1992

Pressure-Based Multigrid Algorithm for Flow at All Speeds

Wei Shyy* and Ming-Hsiung Chen†
University of Florida, Gainesville, Florida 32611
and
Chia-Sheng Sun‡
National Cheng-Kung University, Tainan, Taiwan, Republic of China

A full multigrid/full approximation storage (FMG/FAS) method is developed along with a unified pressure-based algorithm to handle the complex fluid flow problems encompassing both compressible and incompressible regimes. Besides highlighting the key elements of the present algorithm on a curvilinear staggered grid system, several flow problems, ranging from incompressible to hypersonic speeds, are computed, in conjunction with an adaptive grid method, to demonstrate its computational capability. With wide variations in geometry, fluid physics, and grid distribution, speedup between the single- and multigrid procedures can be obtained. Because different pressure boundary conditions are needed for incompressible, subsonic, and supersonic inlet and outlet, the number of grid levels that can be effectively used by the present multigrid method appears flow dependent; the implications of this observation are discussed.

I. Introduction

USE of pressure correction methods for solving incompressible viscous flow problems in Cartesian or cylindrical coordinates is well established, and a number of methods of this type such as SIMPLE,[1,2] SIMPLER,[2] and PISO[3] have been developed. The basic similarity of these methods is that the momentum equations are first solved using a guessed pressure field, resulting in a tentative velocity field. An equation for the pressure corrections is obtained via manipulation of the momentum and continuity equations. This equation is solved to obtain the pressure corrections, and the velocities are then corrected to satisfy the continuity equation. The extension of the SIMPLE algorithm to a general nonorthogonal curvilinear coordinate system has been described in Refs. 4–6 and has been successfully applied to various problems as documented in Ref. 6.

When solving a viscous flow problem using a pressure-based method, the computer time required to solve the pressure (correction) equation is often a sizable fraction of the total computational effort.[7,8] Van Doormaal and Raithby[7] report that this fraction can be as high as 80% of the total CPU time. This observation is also qualitatively confirmed in Ref. 8, which finds that, for high Reynolds number flows, the pressure-correction equation requires many more sweeps of a point-symmetric successive over-relaxation (point-SSOR) or line-SSOR method to converge than either the momentum equation or other scalar transport equations. This is because the pressure-correction equation, which has the form of an anisotropic elliptic equation, is diffusion dominated, whereas the other equations are convection dominated. It is well known that point- and line-iterative methods converge rather slowly on elliptic problems such as the Poisson equation, particularly as the number of mesh points becomes large. To expedite the convergence rates, the multigrid (MG) method[9,10] has been found to be very useful for improving the performance of these single-grid (SG) solvers for elliptic equations. With this motivation, the multigrid procedure has been developed and applied to the solution of the individual transport equations,[11,12] which, in essence, improves the convergence of the pressure equation. However, since it does not account for the coupling among the dependent variables at different grid levels, the improvement of the overall convergence rate is limited.

Miller and Schmidt[13] have combined the SIMPLE algorithm and the multigrid method on a Cartesian grid system to accelerate the convergence to the steady state. They consider the planar driven cavity problem at a Reynolds number of 400 and the axisymmetric contraction flow at a Reynolds number of 968. Modest grid size of 34×34 nodes are employed in both cases and good speedup between the MG and SG procedures reported. Using different approaches, Hortmann et al.[14] and Vanka[15] have computed, respectively, the natural convection in a square cavity and the driven cavity flow using much larger grid sizes. Substantial speedup is observed in both studies. In Ref. 14, a pressure-correction type of sequential solver using the nonstaggered grid system is employed, whereas in Ref. 15 a coupled simultaneous approach directly solving the momentum and mass continuity equations, using the staggered grid system, is devised. All of the studies conducted in Refs. 13–15 adopt the Cartesian grid; they are of limited capabilities to solve the flows in complex configurations.

In a recent work,[16] a multigrid method has been successfully combined with a curvilinear coordinate algorithm suitable for solving an incompressible recirculating flow problem in complex geometries. This combined approach uses a pressure-correction formulation and the so-called full multigrid/full approximation storage (FMG/FAS) technique for solving the whole governing equations at various grid levels. Good speedup ratios from the SG to MG procedure have been obtained for several incompressible recirculating flow problems. In the present work, this FMG/FAS methodology is further developed to solve the flow at all speeds, ranging from incompressible to hypersonic regime. To perform these computations, a generalized pressure-correction algorithm developed earlier[17] is extended to use the multigrid solution method. An adaptive grid procedure is also incorporated into the algorithm to improve the solution accuracy. Several different flow geometries are used to demonstrate the performance of the present approach. For the incompressible cases, two configurations, including a straight channel with a single "bump" mounted on the lower wall and a kidney-shaped channel resembling qualitatively a gas-turbine combustor, have been chosen. For the

Received May 10, 1991; revision received March 5, 1992; accepted for publication March 5, 1992.

*Professor, Department of Aerospace Engineering, Mechanics, and Engineering Science.
†Postdoctoral Research Scholar, Department of Aerospace Engineering, Mechanics, and Engineering Science.
‡Graduate Student, Institute of Aeronautics and Astronautics.

compressible cases, a channel with mounted bump of variable curvatures is computed for inviscid transonic, supersonic, and hypersonic flows.

After the completion of the present work, two papers applying the MG method to solve the flows in complex geometries have been published.[18,19] Together with the present effort, these studies assess the performance of the MG technique using different base algorithms. For the application of the MG algorithm to the density-based method, the paper by Ni[20] and various references cited by Hirsch[21] can be consulted.

II. Pressure-Based Algorithm in Curvilinear Coordinates

The strong conservation-law form of the steady-state Navier-Stokes equation is adopted here, as illustrated in the following:

$$f_x + g_y = \sigma_x + \theta_y + s$$

$$f = (\rho u,\ p + \rho u^2,\ \rho uv)^T \tag{1}$$

$$g = (\rho v,\ \rho vu,\ p + \rho v^2)^T$$

where u and v are the velocity components in the coordinate directions, x and y, respectively, ρ is density, p is pressure, σ and θ represent viscous stress and work terms for each coordinate direction, and s accounts for other source terms such as those arising from the body forces. Upon transforming to ξ, η curvilinear coordinates with the aid of the chain rule for partial derivatives, Eq. (1) becomes

$$\tilde{f}_\xi + \tilde{g}_\eta = \tilde{\sigma}_\xi + \tilde{\theta}_\eta + \tilde{s} \cdot J$$

$$\tilde{f} = y_\eta f - x_\eta g$$

$$\tilde{g} = -y_\xi f + x_\xi g$$

$$\tilde{\sigma} = y_\eta \sigma - x_\eta \theta \tag{2}$$

$$\tilde{\theta} = -y_\xi \sigma + x_\xi \theta$$

$$\tilde{s}(\xi, \eta) = s(x, y)$$

and J is the Jacobian of the inverse transformation

$$J = x_\xi y_\eta - x_\eta y_\xi \tag{3}$$

It is noted that in Eq. (2) the strong conservation-law form has been retained to facilitate the numerical formulation of the conservation principle. It is noted that, since the compressible flow cases are for the inviscid flow with uniform inlet condition, a constant total temperature is sufficient for the energy consideration.

The essence of the pressure-correction algorithm for solving the incompressible flows can be briefly described as follows. Discretization of the momentum and continuity equations yields the following difference equations:

$$([D] - [E])\{Q\} + [B]\{P\} = \{F\} \tag{4a}$$

$$[C]\{V\} = \{G\} \tag{4b}$$

where

$\{Q\}$, $\{P\}$ = vector with nodal value of (u, v) and p, respectively, as its components

$[D]$ = diagonal matrix with positive elements

$[E]$ = matrix with zero entries on its diagonal; difference operator $D - E$ accounts for both the convection and viscous effects

$[B]$ = difference operator for gradient

$[C]$ = difference operator for divergence

$\{F\}$ and $\{G\}$ = explicit forcing function terms from source and boundary conditions

Next, one can formulate a predictor/corrector procedure to iteratively update both the velocity and static pressure fields by splitting $\{Q\}$ and $\{P\}$ into two parts:

$$\{Q\} = \{Q^*\} + \{Q'\} \tag{5a}$$

$$\{P\} = \{P^*\} + \{P'\} \tag{5b}$$

By reformulating the momentum equation, Eq. (4a), to the form of

$$([D] - [E])\{Q^*\} + [B]\{P^*\} = \{F\} \tag{6}$$

one obtains $\{Q\}$ based on a given $\{P\}$. Furthermore, the relationship between the pressure correction and velocity correction can also be derived:

$$([D] - [E])\{Q'\} + [B]\{P'\} = 0 \tag{7}$$

Here, the SIMPLE algorithm takes a simplified form of Eq. (7) to link $\{Q'\}$ and $\{P'\}$, namely,

$$[D]\{Q'\} + [B]\{P'\} = 0 \tag{8}$$

Similarly, the continuity equation can be written as

$$[C]\{Q'\} = \{G\} - [C]\{Q^*\} \tag{9}$$

Hence, a pressure correction equation for incompressible flow can be derived by combining Eqs. (8) and (9):

$$[C][D]^{-1}[B]\{P'\} = [C]\{Q^*\} - \{G\} \tag{10}$$

For highly compressible flows, the density is a strong function of pressure. Therefore, in the formulation of the pressure-correction equation, it is necessary to correct both the density and velocity fields simultaneously to satisfy the continuity equation. This practice holds a key to successfully solve the compressible flow problems. Each flux term in the continuity equation can be decomposed into four parts, e.g.,

$$\rho U = (\rho^* + \rho')(U^* + U')$$

$$= \underset{1)}{\rho^* U^*} + \underset{2)}{\rho^* U'} + \underset{3)}{\rho' U^*} + \underset{4)}{\rho' U'} \tag{11}$$

where U is the contravariant velocity along the ξ direction. These four terms represent 1) the mass flux calculated based on the given density and velocity fields, 2) the contribution from the velocity corrections, 3) the linear contribution from the density corrections stemming from the compressibility effect, and 4) the nonlinear contribution from the compressibility effect, respectively.

It is useful to examine the relative importance of the various terms as a function of the Mach number. The combination of terms 1 and 2 leads to the incompressible form of the pressure-correction equation given earlier. With the aide of equation of state and definition of Mach number, the velocity correction term $\rho^* U'$ is found to be inversely proportional to the local Mach number M_a, i.e.,

$$\rho^* U' \sim \frac{1}{M_a \sqrt{T}} p'_\xi \tag{12a}$$

$$\rho^* V' \sim \frac{1}{M_a \sqrt{T}} p'_\eta \tag{12b}$$

The equation of state for an ideal gas can be written as

$$\rho = C^\rho P \tag{13}$$

where

$$C^{\rho} = 1/RT$$

Hence, the density correction ρ' can be expressed as

$$\rho' = C^{\rho} p' \tag{14}$$

Whereas $\rho^* U'$ contributes a diffusion term to the pressure-correction equation, $\rho' U^*$ contributes a convection-like term. This occurs because the velocity correction is proportional to the gradient of the pressure correction, whereas the density correction is proportional to the pressure correction directly. Since ρ is inversely related to T, the contribution of $\rho' U^*$ to the pressure-correction equation is found to be proportional to the local Mach number, i.e.,

$$\rho' U^* \sim \frac{M_a}{\sqrt{T}} p' \tag{15}$$

Hence it is clear that the ratio of 3 to 1 in Eq. (11) is proportional to the square of local Mach number; this characteristic explains why by omitting 3 and 4 in Eq. (11) the original SIMPLE algorithm works well for incompressible flows but not for high-speed flows. The nonlinear correction term $\rho' U'$ is independent of the Mach number by the same arguments. Since neither ρ' nor U' is necessarily small during the early iterations, it is useful to include these terms explicitly in the source term of the pressure correction equation to help stabilize the computational procedure.

The major remaining issue is how to interpolate the transport coefficients as well as the p' values at the control volume face for the pressure-correction equation. Because of the convection-diffusion nature of the pressure-correction equation for compressible flow, a two-point average does not guarantee the positiveness of the coefficients, and hence the criterion for the numerical stability of an iterative solution procedure may be violated. It is important to note that it is the accuracy of the divergence of the mass flux calculation, namely, the terms such as $\rho^* U^*$, that determines the accuracy of the pressure field. The formulation of the other pressure-correction terms does not affect the final solution accuracy; however, they can critically affect the numerical stability. Based on this realization, one can devise any suitable approximation for the pressure-correction terms to expedite the convergence rate. In the present work, two approximations have been constructed. First, based on the local Mach number, the values at the control volume faces are taken as either two-point central average (for low M_a) or one-sided upwind value (for high M_a). The switch point of the interpolation formulas is found to be necessarily subsonic; however, the convergence path is not sensitive to the change of the switch point as long as a converged solution can be obtained. Second, for the subsonic cases, the convection part of the transport equation for the pressure correction is linearly weighted according to the local Mach number. These procedures have been found to be effective in yielding stable convergence. As to the nonlinear contribution from the compressibility effect, part 4 in Eq. (11), the present algorithm treats it as an explicit source term with the same switch criterion of interpolation formula adopted, as discussed earlier. This treatment of the nonlinear term is useful in supersonic flow cases, preventing early divergence of the algorithm that may occur otherwise.

For the discretization processes, the convection terms are represented by the second-order upwind scheme[22] whereas all other terms are represented by the second-order central difference schemes. With regard to the boundary conditions, for the incompressible recirculating flows, a no-slip condition is enforced on the wall and a first-order extrapolation is adopted as the outflow boundary condition for u and v velocities along the streamwise ξ direction. No pressure boundary condition is needed for either inflow or outflow boundary. For the compressible inviscid flows, the inlet Mach number (M_{in} and the gas temperature are prescribed. Zero normal mass flux conditions are imposed on the solid walls. For a subsonic outflow, the static pressure is prescribed, and a first-order extrapolation is adopted for the velocity variables. For a supersonic outflow, the same first-order extrapolation is also used for the velocity variables whereas the pressure there is determined by the continuity equation.

III. Multigrid Methodology

In the MG method the computation is carried out on a series of grids G_k with the corresponding solution vector $\{\psi_k\}$ where $k = 1, 2, 3, \ldots, M$, with $k = M$ representing the finest mesh, and the meshes become coarser as the value of k becomes smaller. The exact solution for any variable ψ_k on grid G_k satisfies the following equation:

$$[\alpha_k]\{\psi_k\} = \{\zeta_k\} \tag{16}$$

where $[\alpha_k]$ and $\{\zeta_k\}$ are, respectively, the coefficient matrix and the source term vector derived directly from the discretization procedure adopted. Hence, at convergence, $[\alpha_k]$ and $\{\zeta_k\}$ are based on the exact solutions on grid G_k of the coupled variables. Before convergence, however, they are estimated based on the intermediate solution, and they are continuously updated in the course of iteration.

A. Full Approximation Storage (FAS) Scheme

There are several algorithms for implementing the MG idea, each with several possible variations. One of the simplest is the correction storage (CS) scheme, which is most useful for the linear problems. In this scheme, the calculation starts on the finest grid G_M, and an approximate solution to Eq. (16) is computed by a relaxation method. Unless the approximate solution $\{\phi_k\}$ satisfies Eq. (16) and the boundary conditions, there will be a residual vector $\{R_k\}$ given by

$$[A_k]\{\phi_k\} = \{S_k\} - \{R_k\} \tag{17}$$

where $[A_k]$ and $\{S_k\}$ are based on the intermediate solution $\{\phi_k\}$ without being updated along with $\{\phi_k\}$. A few iterations are performed on grid G_k until the rate of reduction of the residuals falls below a desired level. The residuals are then transferred by a "restriction (or injection)" operator to the next coarser grid G_{k-1} and a correction vector $\{\delta\phi_{k-1}\}$ is obtained by solving the following equations:

$$[A_{k-1}]\{\delta\phi_{k-1}\} = \{I_k^{k-1} R_k\} \tag{18}$$

where I_k^{k-1} is the restriction operator that performs the task of transmitting the information from a fine grid to a coarse grid. Once Eq. (18) is solved, the correction vector $\{\delta\phi_{k-1}\}$ is "prolongated (or interpolated)" to grid G_k and $\{\phi_k\}$ is subsequently corrected as

$$\{\phi_k^{\text{new}}\} = \{\phi_k^{\text{old}}\} + I_{k-1}^{k}\{\delta\phi_{k-1}\} \tag{19}$$

where I_{k-1}^{k} is the prolongation operator. This process of relaxation, restriction, and prolongation is repeated until the desired accuracy on the finest grid G_M is achieved.

The scheme just described serves to illustrate the idea of the multigrid procedure but is inadequate for nonlinear problems such as the Navier-Stokes equations. Since it depends on the linearity of $[\alpha]$ to derive the residual for computing the correction $\{\delta\phi\}$ on the coarse grid, it does not work well for the flow problems of strong nonlinear convection effect. To remedy this deficiency, the so-called full approximation storage (FAS) scheme has been developed,[9] as will be briefly described next.

Without assuming linearity, the fine-grid residual equation

$$[\alpha_k]\{\phi_k + \delta\phi_k\} - [A_k]\{\phi_k\} = \{\zeta_k\} - \{S_k\} + \{R_k\} \tag{20}$$

can be written on the coarse grid by restricting the residual to form a corresponding equation

$$[\alpha_{k-1}]\{\hat{I}_k^{k-1}\phi_k + \delta\phi_{k-1}\} - [A_{k-1}]\{\hat{I}_k^{k-1}\phi_k\} = \{\zeta_{k-1}\} - \{S_{k-1}\} + \{I_k^{k-1}R_k\} \quad (21)$$

putting the known quantities on the right-hand side reduces Eq. (21) to

$$[\alpha_{k-1}]\{\psi_{k-1}\} = \{\xi_{k-1}\} \quad (22)$$

where

$$\{\psi_{k-1}\} = \hat{I}_k^{k-1}\{\phi_k\} + \{\delta\phi_{k-1}\} \quad (23)$$

and

$$\{\xi_{k-1}\} = \{\zeta_{k-1}\} + [A_{k-1}]\{\hat{I}_k^{k-1}\phi_k\} - \{S_{k-1}\} + \{I_k^{k-1}R_k\} \quad (24)$$

Here, $\hat{I}_k^{k-1}$ for $\{\phi_k\}$ may be different from the residual transfer operator I_k^{k-1} for $\{R_k\}$, although they are taken to be the same in the present work. This is known as the FAS scheme, since from Eq. (22) on the coarse grid the complete solution $\{\psi_{k-1}\}$, not just the correction $\{\delta\phi_{k-1}\}$, is computed. After solving Eq. (22), the fine-grid solution is updated via

$$\{\phi_k^{\text{new}}\} = \{\phi_k^{\text{old}}\} + I_{k-1}^k(\{\phi_k^{\text{new}}\} - I_k^{k-1}\{\phi_k^{\text{old}}\}) \quad (25)$$

which represents interpolating the approximate correction $\{\delta\phi_{k-1}\}$ and adding to the intermediate solution $\{\phi_k\}$ on fine grid G_k. Since the starting values for $\{\phi_{k-1}\}$ are $\hat{I}_k^{k-1}\{\phi_k\}$, the source terms $\{\zeta_{k-1}\}$ and $\{S_{k-1}\}$ are identical in the first coarse-grid iteration. All of the right-hand side terms in Eq. (24), except $\{\zeta_{k-1}\}$, are calculated once and then kept unchanged during subsequent iterations on the coarse grid; they appear as extra explicit source terms with prescribed values. With FAS, the source term and the coefficient matrix on the coarse grid can be continuously updated to reflect progress made to the dependent variables. Since both $[\alpha]$ and $\{\zeta\}$ can be strongly dependent on $\{\psi\}$ in nonlinear manners, this feature is very helpful.

B. Full Multigrid Algorithm

When using multigrid cycles as a solution method, one starts with an initial approximation $\{\phi_k\}$ on the finest grid G_M. If a good initial approximation can be made, then fewer cycles will be required to solve the problem. To get a better first approximation, one can interpolate an approximate solution from a coarser grid through a coarse-to-fine grid transfer operator, namely,

$$\{\phi_k\}_{\text{initial}} = \Pi_{k-1}^k\{\phi_{k-1}\}_{\text{initial}} \quad (26)$$

where Π_{k-1}^k is a coarse-to-fine grid transfer operator that need not be the same as I_{k-1}^k in Eq. (19). Starting with an approximate solution on the coarsest grid G_1, a sufficiently large number of relaxation sweeps can be taken to give an accurate solution there. This solution is then interpolated onto the next finer grid G_2 by the prolongation operator and used as a starting guess for the first V-cycle multigrid procedure; this two-grid V-cycle procedure continues till it meets the local convergence criterion on G_2. After the convergence on G_2 is attained, the solution $\{\phi_2\}$ is then interpolated onto next finer grid, G_3, initiating a new three-grid V-cycle relaxation involving G_1, G_2, and G_3, until convergence is attained on G_3. This process is repeated by interpolating the solution from G_{k-1} to G_k as a first approximation, and solving the problem by a V-cycle iteration, until the final converged solution is obtained on the finest grid G_M. The aforementioned solution process is termed the full multigrid (FMG) procedure, which is important for obtaining fast convergence.

C. Multigrid Cycling

With the FMG-FAS algorithm, multigrid codes differ in their cycling procedures, which can be either fixed or adaptive, that is, the decisions of when to switch grids and which direction to go (i.e., to a coarser or finer grid) can be either prescribed in advance or made internally as the numerical solution develops.

With a coupled nonlinear system of equations, the rate of convergence of the various equations may be substantially different. For example, it is demonstrated in Ref. 5 that for a high Reynolds number flow the pressure equation is much harder to converge than other linearized transport equations because of its stronger diffusion characteristics. In a decoupled algorithm where all of the variables are sequentially updated, an adaptive cycling algorithm is not necessary for any of these convection-dominated equations because of their very good convergence rates. With this realization, a fixed cycling algorithm is used in the present work for simplicity. As will be demonstrated later, this fixed cycling algorithm is also very robust. Specifically, in the present work, fixed ν_r iterations before applying restriction and ν_p iterations after prolongation in the V-cycle are used. The MG cycling is terminated only in the finest grid when a certain prescribed criterion is reached. A schematic illustration of the V-cycle fixed MG procedure, along with the values of ν_r and ν_p on each grid level, adopted in the present work are given in Fig. 1. The optimum choice of the cycling procedure is problem dependent; however, the increasing number of sweeps conducted at the coarser grid levels is quite tolerable since the computing effort per iteration is reduced geometrically as the grid is coarsened because of the smaller number of unknowns, which reduces the CPU time per iteration, and the associated improvement in the convergence rate, which reduces the number of iterations required for reaching the same convergence criteria.

D. Restriction and Prolongation in Staggered Grid

In the present work, a staggered grid is employed for the velocity components and the pressure. Figure 2a illustrates the basic staggered grid notation in both single- and multi-grid systems. Relationships of the velocity and pressure control volumes between the fine and coarse grids are depicted in Fig. 2b. Although the basic concepts of prolongation and restriction remain the same, the actual forms of the transfer operators are different for each of the variables u, v, and p, as well as the corresponding residuals R^u, R^v, and R^p. In the present work, the restrictions are made by averaging the nearby fine grid values, and the prolongation by applying bilinear interpolation from the coarse grid values. Both the restriction and interpolation are conducted through area weighted procedures. For the compressible flows, the temperature and density fields can be directly computed based on the constant total temperature and the equation of state, respectively, at every grid level; they do not need to be restricted or prolongated from the current grid level to the next grid level.

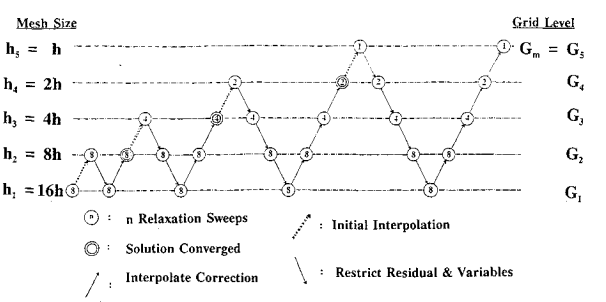

Fig. 1 Full multigrid (FMG) procedure with fixed V cycles, $M = 5$ grid levels.

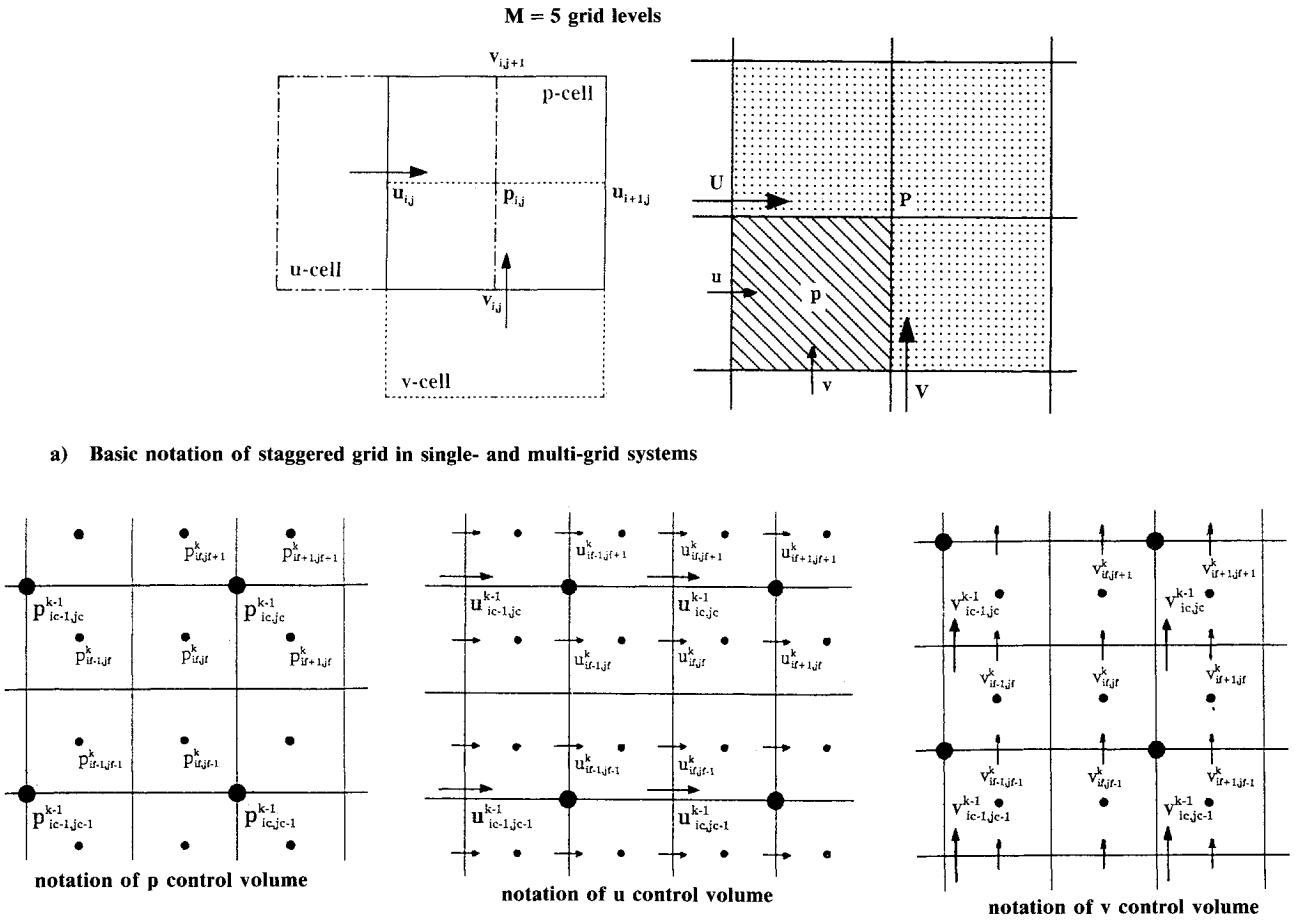

a) Basic notation of staggered grid in single- and multi-grid systems

b) Relationship of velocities and pressure control volumes between coarse and fine grid systems

Fig. 2 Schematic of staggered grid layout and control volume arrangement for both single- and multi-grid systems.

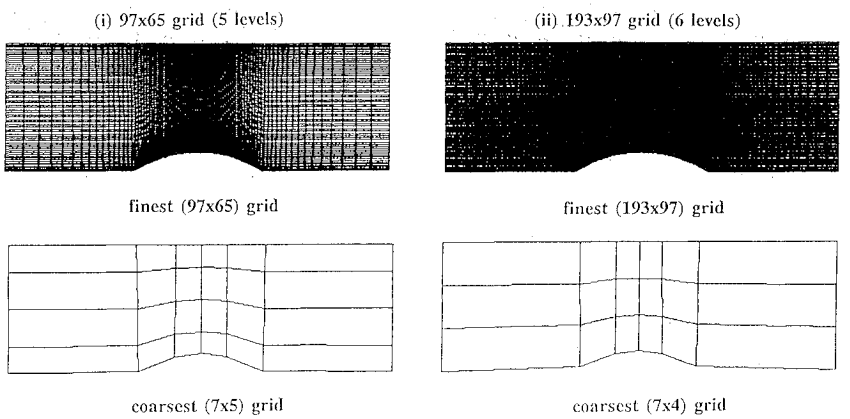

Fig. 3 Finest and coarsest grid systems of the incompressible channel flow employed in the MG procedure.

IV. Results and Discussion

A. Incompressible Flows

Several recirculating flow problems with different geometries as well as Reynolds numbers have been computed to assess the performance of the present pressure-based FMG/FAS algorithm. The first flow configuration is a straight channel with a circular bump mounted in the middle of the lower wall. The height-to-length ratio of the channel is 1 to 3, and the maximum height of the bump is 15% of the inlet height. Figure 3 shows the finest and the coarsest levels of the grid system employed by the MG technique; with the 97×65 grid system, a five-level MG procedure with 7×5 nodes at the coarsest level is employed, whereas with the 193×97 grid system a six-level MG procedure also with 7×4 nodes at the coarsest level is employed. The Navier-Stokes equations with identical boundary conditions as well as appropriate source modifications needed by the MG method are solved at every grid level. The FMG/FAS procedure, in a V-cycle as illustrated in Fig. 1, is conducted successively back and forth at these grid levels. Two Reynolds numbers based on the inlet condition, 10^2 and 10^3, are used. A uniform velocity distribution is taken at the inlet.

The streamlines and pressure contours are depicted in Fig. 4 for the case of $Re = 10^3$. A sizable separation zone is present in the rear region of the bump. The convergence paths of both SG and MG procedures with $Re = 10^2$ and 10^3, based on the outer iterations conducted at the finest grid levels, are shown

in Fig. 5. In all computations, identical numbers of LSOR sweeps as well as the relaxation factors are adopted at each grid level. The convergence paths are represented in terms of the absolute residuals of the u-momentum equation, summed over all of the finite volumes at the finest grid level and normalized by the total incoming momentum flux. Several interesting features are revealed by Fig. 5. Obviously the MG procedure yields substantially faster convergence rates than the SG procedure; as the number of grids increases at the finest level, the MG procedure becomes more superior to the SG procedure, achieving an order of magnitude speedup in convergence rate on the finest grid level for $Re = 10^2$. Furthermore, although the Reynolds number and the grid size noticeably affect the performance of the SG procedure, they exert virtually no impact on the MG procedure.

The estimation of the speed-up ratios in terms of CPU time is less straightforward, of course, because of the way the computer program is structured, the computer architecture employed, the cycling procedure and the number of inner/outer iterations used at every grid level of the MG algorithm, and the control criteria imposed on the initial computation of the FMG procedure before reaching the finest grid level. Not many papers dealing with the MG algorithm give adequate information in this regard. Reference 16 has provided a summary of the various aspects of the performance comparison between the SG and MG procedures. For all of these cases discussed in the present work, the ratio of the CPU time between the SG and MG algorithms is about 1.6–2.1 times the corresponding ratio of the number of iterations at the finest grid level, which is generally consistent with that documented in Ref. 16. This range is also comparable to that given by Hortmann et al.[14] for the natural convection problem with a Rayleigh number of 10^5. However, a recent work of Rayner[18] indicates a far greater discrepancy between the ratio of fine-grid convergence rate of SG and MG procedures and the corresponding CPU time ratio. These differences indicate that the relative performance among different approaches cannot be assessed based on the nominal convergence rate alone. As already pointed out, in our algorithm, the number of iterative sweeps needed for each discretized individual equation to achieve the same convergence criterion at the coarser grid level is smaller than that at the finest grid level because of the reduced number of unknowns at the coarser grid levels. Hence, the ratio of work units to the number of fine grid iterations can be lower than that indicated by Fig. 1.

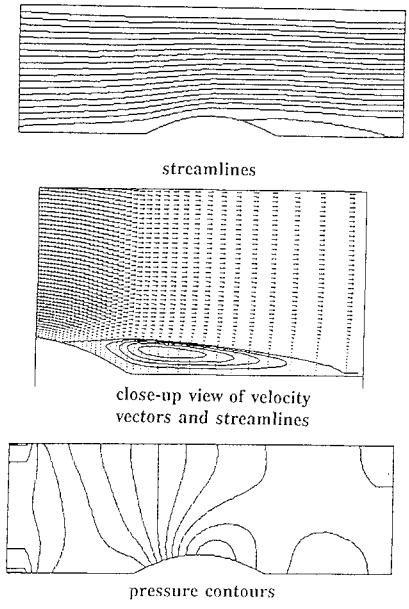

Fig. 4 Solutions of incompressible flow with $Re = 10^3$.

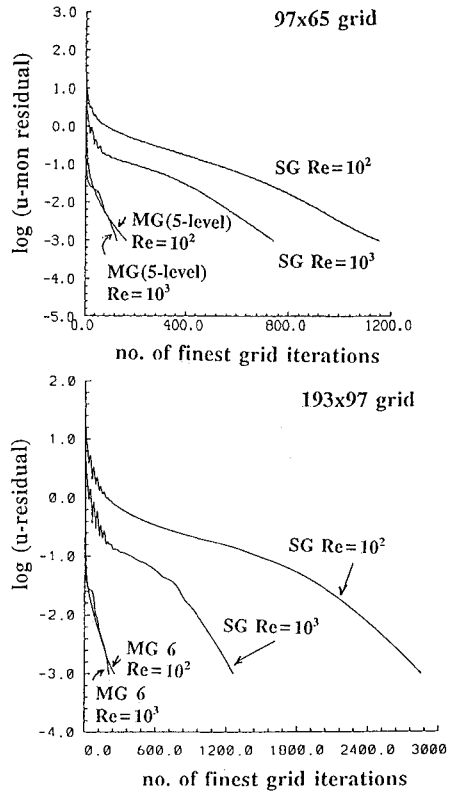

Fig. 5 Convergence paths of SG and MG procedures of incompressible channel flows with $Re = 10^2$ and 10^3.

Next, a kidney-shaped two-dimensional channel is used as the test configuration, which exhibits greater degrees of geometrical complexities. The dump regions downstream of the inlet produce substantial flow recirculations; these recirculating eddies can strongly affect the curvatures of the main incoming flow. The case chosen here is for an inlet Reynolds number of 6.2×10^3, and a uniform incoming velocity profile, and constant fluid properties. This high value of Reynolds number is used primarily for testing the performance of the MG procedure for a strongly convection-dominated flow in a complex configuration. This flow configuration has been used before to aid the development of the SG curvilinear coordinate algorithm (see Refs. 4 and 5).

Figure 6a shows the original grid systems of the kidney-shaped channel displayed at the finest (97×49 nodes) and the coarsest (7×4 nodes) grid levels. To help optimize the grid distribution, an adaptive grid computational technique[17] has been used. The resulting adaptive grid systems at the five corresponding grid levels are shown in Fig. 6b. The adaptive grid system is generated at the finest grid level according to the solutions obtained on the original grid. Successive grid coarsening is then conducted at different levels to aid the MG procedure. It is striking to observe that, as demonstrated in Fig. 6, the wide differences in grid as well as geometrical characteristics exist at different grid levels. It is remarkable that, with a much degraded geometrical resolution at the coarsest grid level, the MG procedure can still exhibit an improved convergence rate; this demonstrates the robustness of the MG algorithm devised.

Figure 7 depicts the streamlines and pressure contours obtained on the adaptive grid for the case of $Re = 6.2 \times 10^3$, where complicated solution characteristics are exhibited. Figure 8 compares the convergence paths of an SG procedure on a 97×49 original grid and two MG procedures, one on the original grid and the other on the adaptive grid. By optimizing the grid distribution according to the solution characteristics, the adaptive grid technique can help improve both the convergence rate and the numerical accuracy.

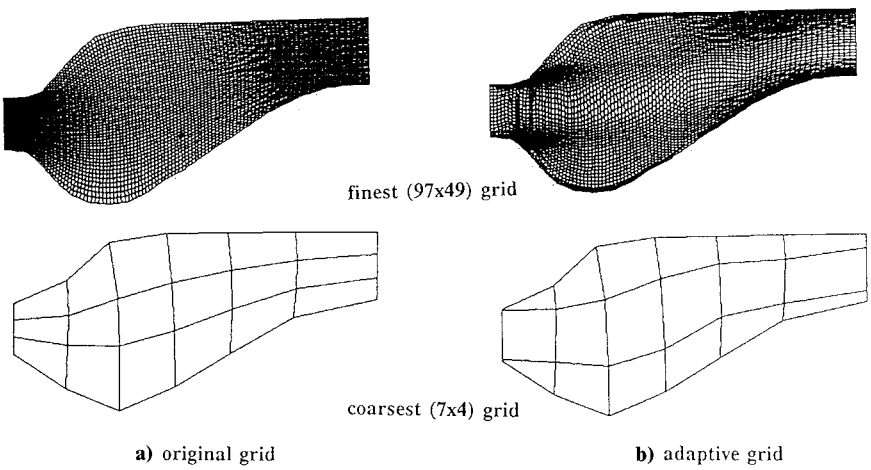

Fig. 6 Finest and coarsest levels of grid systems of the kidney-shaped channel.

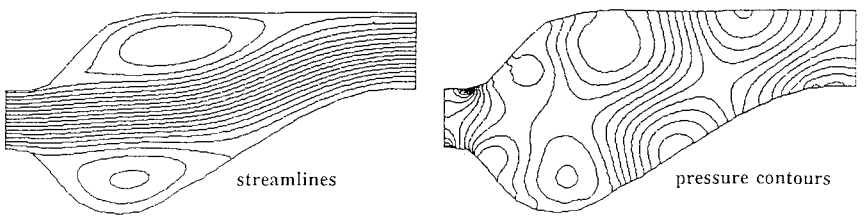

Fig. 7 Solutions of incompressible kidney-shaped channel flow with $Re = 6.2 \times 10^3$.

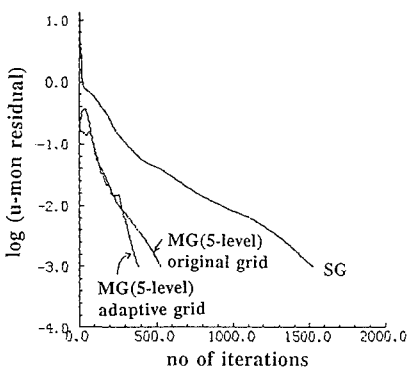

Fig. 8 Convergence paths of SG and MG procedures of incompressible kidney-shaped channel flow with $Re = 6.2 \times 10^3$.

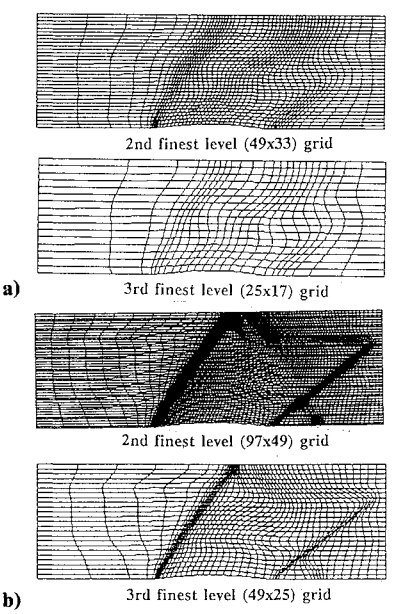

Fig. 9 Adaptive grid systems of a) 97×65 nodes and b) 193×97 nodes, of a channel with 4% bump.

B. Compressible Flows

Next, the present pressure-based FMG/FAS algorithm is applied to solve the inviscid supersonic, hypersonic, and transonic flows in a channel with a bump mounted on the lower wall. For the supersonic flow, the case considered is for an incoming Mach number M_{in} of 1.4 in a channel with 4% bump height. The same channel configuration is also used to compute a hypersonic flow of $M_{in} = 5$. For the transonic flow, it is for an incoming Mach number of 0.675 over a 10% bump. These configurations have been used by many researchers as test problems. For example, Ni[20] has used them to develop a multigrid solver in the context of the density-based compressible flow algorithm. Here, two grid sizes, one with 97×65 nodes and the other with 193×97 nodes, are used in conjunction with the adaptive grid technique. The supersonic flow case is presented first. Figure 9 depicts the different grid levels used by the MG procedure for both the 97×65 and 193×97 grid systems. With the grid adaptation, it is found that, with the nodal distributions shown in Fig. 9, one can only successfully employ a three-level MG procedure; the algorithm fails if four or more grid levels are used. The reason for this seemingly more restricted applicability of the MG method can be found by observing that, because of the strong gradients around the shock, more grid points are clustered there; consequently, the region in front of the bump has only a modest number of nodes. Hence, after two levels of grid coarsening, only a couple of grid lines line between the channel inlet and the bump. For the present cell-centered staggered grid, a prescribed pressure level is needed for the nodes next to the inlet and the three-level grid appears to be the upper limit for an

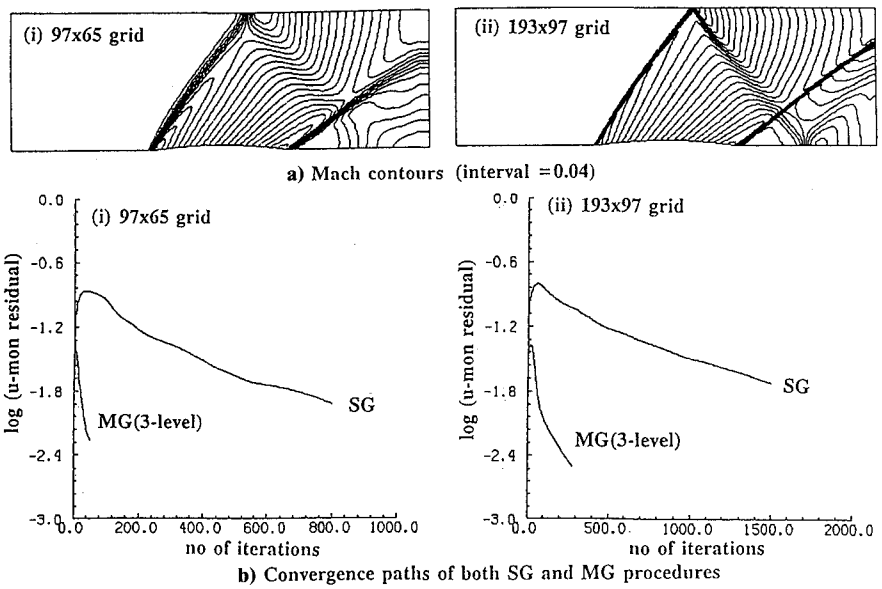

Fig. 10 Mach contours and convergence paths of flow with inlet $M = 1.4$, in a channel with 4% bump.

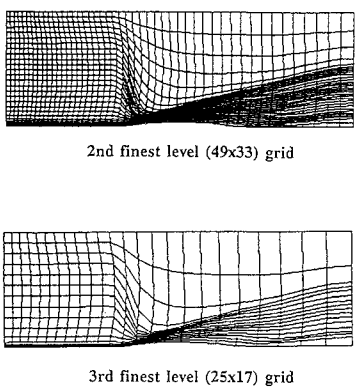

Fig. 11 Adaptive grid system of 97×65 nodes of flow with inlet $M = 5$, in a channel with 4% bump.

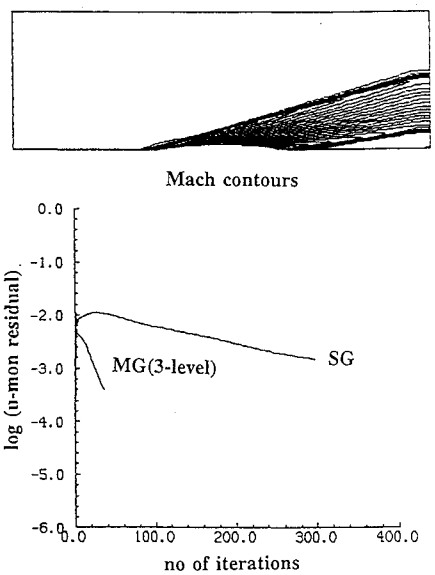

Fig. 12 Mach contours and convergence paths of flow with inlet $M = 5$, in a channel with 4% bump.

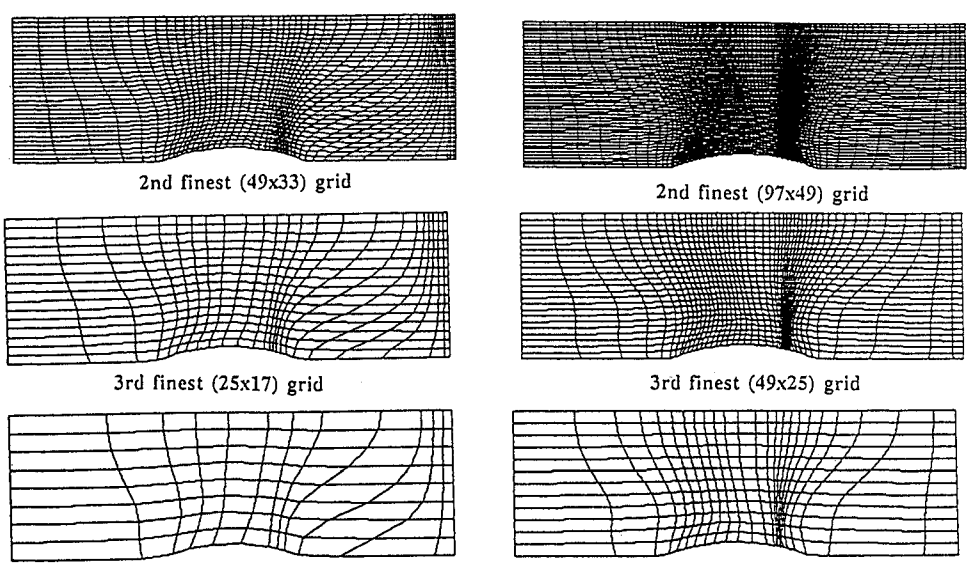

Fig. 13 Grid systems of a) 97×65 nodes and b) 193×97 nodes, of a channel with 10% bump.

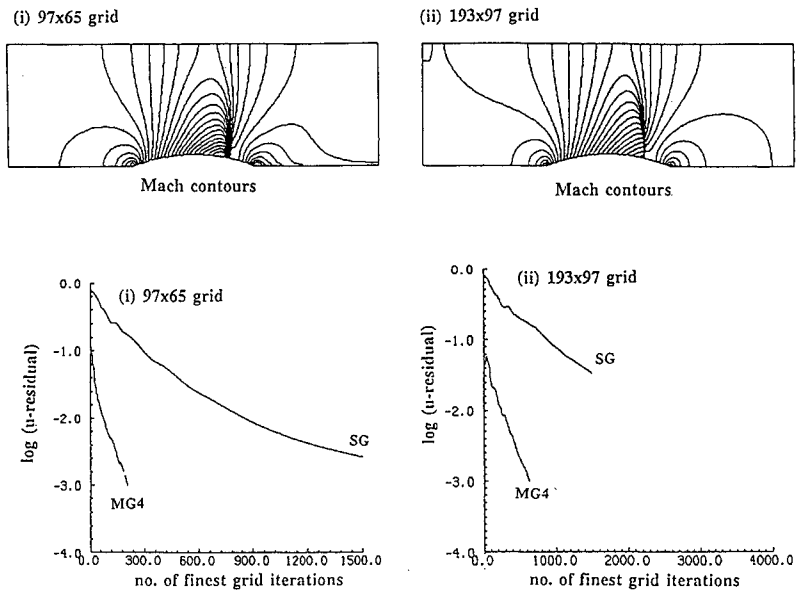

Fig. 14 Mach contours and convergence paths of flow with inlet $M = 0.675$, in a channel with 10% bump.

MG solver to successfully operate with the grid distributions shown in Fig. 9. With one more level of grid coarsening, the first unknown pressure node will have a control volume occupying almost the whole region between the channel inlet and the bump, and the algorithm can no longer work well. It is clear that a balance must be maintained between the nonuniform clustering of the finest grid system desired by the accuracy aspect and the minimum resolution of the coarsest grid system required by the MG procedure.

Figure 10 displays the computed Mach number contours as well as the convergence paths of the SG and MG procedures with $M_{in} = 1.4$ for the adaptive grid systems. Obviously, as the grid refinement is made along with the grid adaptation, sharper solution characteristics emerge. For both cases, the speed-up ratios between the three-level MG procedure and the SG procedure are substantial, demonstrating the effectiveness of the present pressure-based FMG/FAS solver.

Next, a hypersonic flow case of $M_{in} = 5$ in the same 4% bump channel is presented. For this flow problem, the shocks formed at the front and rear of the bump are of high oblique angles; they do not impinge on the top wall in the domain considered. To accommodate this feature, as shown in Fig. 11, the grid adaptation is conducted more along the η direction. Figure 12 shows the Mach contours as well as the convergence paths. Substantial speedup is again obtained from the SG to three-level MG method. It is also noted that, because the pressure correction equation is of a stronger convection characteristic here, it can converge faster with a prescribed velocity field. Figure 12 illustrates that at $M_{in} = 5$ the overall convergence rates of both the SG and MG methods are faster than the previous case with a lower inlet Mach number, $M_{in} = 1.4$.

Finally, a transonic case with an inlet Mach number of 0.675 over a 10% bump is presented in the following. For this flow, since the outflow condition is subsonic, outlet pressure must be specified. It appears that the effect of the boundary treatment on the allowable level of the MG procedure is also pronounced. For a supersonic inlet, the nature of the flow does yield a uniform pressure field in region upstream of the bump. For the present transonic case, the elliptic nature of the subsonic outflow condition causes nonuniform pressure distributions near the outlet. Figure 13 shows adaptive grid systems of 97×65 and 193×97 nodes at different multigrid levels, used by the MG scheme. For the present case, a four-level MG procedure can yield convergent solutions; however, the difference in performance between the three-level and four-level MG procedures is not much. The Mach number contours and the convergence paths of the SG and MG procedures computed with both grid systems are depicted in Fig. 14. Again, as the grid is refined along with adaptation, the solutions are improved whereas the relative advantage of the MG procedure in convergence rate becomes higher.

V. Summary and Conclusion

A pressure-based FMG/FAS procedure is developed and applied in conjunction with an adaptive grid method for fluid flows ranging from incompressible to hypersonic speed. With wide variations in geometry, fluid physics, and grid size, substantial speedup between the MG and SG procedures can be consistently observed. For the incompressible flows, since the present staggered grid system does not need prescription of the inflow or outflow pressure boundary condition, a robust performance of the MG procedure is attained. It is demonstrated that, even with significant degradation of the geometric resolution at coarser grid levels, effective smoothing can still be performed there. Consequently, the MG method can operate successfully with very few grid points at the coarsest level.

For the compressible flows, because of the need to specify either the inlet pressure (for a supersonic inlet) or the outlet pressure (for a subsonic outlet), there appears to be a more stringent limit of the allowable number of grid levels of the MG procedure than for the incompressible flows. This limit depends, of course, on the characteristics of grid distribution, flow configuration, and number of grid points employed. However, even with such a limit of the number of grid levels, sizable speed-up ratios can still be attained, demonstrating that the present algorithm is capable of yielding solutions with improved efficiencies for a variety of flows within a unified numerical framework.

Acknowledgment

The authors are grateful to acknowledge that some of the computations were made using CRAY-YMP of the National Center for Supercomputer Applications (NCSA) at the University of Illinois through a research grant.

References

[1]Patankar, S. V., and Spalding, D. B., "A Calculation Procedure for Heat, Mass and Momentum Transfer in Three-Dimensional Parabolic Flows," *International Journal of Heat and Mass Transfer*, Vol. 15, 1972, pp. 1787–1806.

[2]Patankar, S. V., *Numerical Heat Transfer and Fluid Flow*, Hemisphere, Washington, DC, 1980.

[3]Issa, R. I., "Solution of the Implicitly Discretized Fluid Flow

Equations by Operator-Splitting," *Journal of Computational Physics,* Vol. 62, 1986, pp. 40–65.

[4]Shyy, W., Tong, S. S., and Correa, S. M., "Numerical Recirculating Flow Calculation Using a Body-Fitted Coordinate System," *Numerical Heat Transfer,* Vol. 8, 1985, pp. 99–113.

[5]Braaten, M. E., and Shyy, W., "A Study of Recirculating Flow Computation Using Body-Fitted Coordinates: Consistency Aspects and Mesh Skewness," *Numerical Heat Transfer,* Vol. 9, 1986, pp. 559–574.

[6]Shyy, W., and Vu, T. C., "On the Adoption of Velocity Variable and Grid System for Fluid Flow Computation in Curvilinear Coordinates," *Journal of Computational Physics,* Vol. 92, 1991, pp. 82–105.

[7]Van Doormaal, J. P., and Raithby, G. D., "Enhancement of the SIMPLE Method for Prediction Incompressible Fluid Flows," *Numerical Heat Transfer,* Vol. 7, 1984, pp. 147–163.

[8]Shyy, W., and Braaten, M. E., "Three-Dimensional Analysis of the Flow in a Curved Hydraulic Draft Tube," *International Journal for Numerical Methods in Fluids,* Vol. 6, 1986, pp. 861–882.

[9]Brandt, A., "Multi-Level Adaptive Solutions to Boundary Value Problems," *Mathematics of Computation,* Vol. 31, 1977, pp. 333–390.

[10]Hackbusch, W., and Trottenberg, U. (eds.), *Multigrid Methods,* Lecture Notes in Mathematics, Vol. 960, Springer-Verlag, Berlin, 1982.

[11]Hutchinson, B. R., and Raithby, G. D., "A Multigrid Method Based on the Additive Correction Strategy," *Numerical Heat Transfer,* Vol. 9, 1986, pp. 511–538.

[12]Rhie, C. M., "A Pressure Based Navier-Stokes Solver Using the Multigrid Method," AIAA Paper 86-0207, 1986.

[13]Miller, T. F., and Schmidt, F. W., "Evaluation of a Multilevel Technique Applied to the Poisson and Navier-Stokes Equations," *Numerical Heat Transfer,* Vol. 13, 1988, pp. 1–26.

[14]Hortmann, M., Peric, M., and Scheuerer, G., "Finite Volume Multigrid Prediction of Laminar Natural Convection: Benchmark Solutions," *International Journal for Numerical Methods in Fluids,* Vol. 11, 1990, pp. 189–207.

[15]Vanka, S. P., "Block-Implicit Calculation of Navier-Stokes Equations in Primitive Variables," *Journal of Computational Physics,* Vol. 65, 1986, pp. 138–158.

[16]Shyy, W., and Sun, C.-S., "Development of a Pressure-Correction/Staggered-Grid Based Multigrid Solver for Incompressible Recirculating Flows," Technical Rept., Dept. of Aerospace Engineering, Mechanics and Engineering Science, Univ. of Florida, Gainesville, FL, 1991.

[17]Shyy, W., and Braaten, M. E., "Adaptive Grid Computation for Inviscid Compressible Flows Using a Pressure Correction Method," AIAA Paper 88-3566-CP, 1988.

[18]Rayner, D., "Multigrid Flow Solutions in Complex Two-Dimensional Geometries," *International Journal for Numerical Methods in Fluids,* Vol. 13, 1991, pp. 507–518.

[19]Joshi, D. S., and Vanka, S. P., "Multigrid Calculation Procedure for Internal Flows in Complex Geometries," *Numerical Heat Transfer,* Vol. 20, 1991, pp. 61–80.

[20]Ni, R. H., "A Multiple Grid Scheme for Solving the Euler Equations," *AIAA Journal,* Vol. 20, 1982, pp. 1565–1571.

[21]Hirsch, C., *Numerical Computation of Internal and External Flows,* Vol. 2, Wiley, New York, 1990.

[22]Shyy, W., Thakur, S., and Wright, J., "Second-Order Upwind and Central Difference Schemes for Recirculating Flow Computation," *AIAA Journal,* Vol. 30, No. 4, 1992, pp. 923–932.